Gravity capillary waves in fluid layers under normal electric fields

Demetrios T. Papageorgiou* and Peter G. Petropoulos†
Department of Mathematical Sciences, New Jersey Institute of Technology, University Heights, Newark, New Jersey 07102, USA

Jean-Marc Vanden-Broeck‡
School of Mathematics, University of East Anglia, Norwich NR4 7TJ, United Kingdom
(Received 6 June 2005; published 1 November 2005)

We study the formation and dynamics of interfacial waves on a perfect dielectric ideal fluid layer of finite depth, wetting a solid wall, when the region above the fluid is hydrodynamically passive but has constant permittivity, for example, air. The wall is held at a constant electric potential and a second electrode having a different potential is placed parallel to the wall and infinitely far from it. In the unperturbed state the interface is flat and the normal horizontally uniform electric field is piecewise constant in the liquid and air. We derive a system of long wave nonlinear evolution equations valid for interfacial amplitudes as large as the unperturbed layer depth and which retain gravity, surface tension and electric field effects. It is shown that for given physical parameters there exists a critical value of the voltage potential difference between electrodes, below which the system is dispersive and above which a band of unstable waves is possible centered around a finite wavenumber. In the former case nonlinear traveling waves are calculated and their stability is studied, while in the latter case the instability leads to thinning of the layer with the interface touching down in finite time. A similarity solution of the second kind is found to be dominant near the singularity, and the scaling exponents are determined using analysis and computations.

DOI: 10.1103/PhysRevE.72.051601 PACS number(s): 68.15.+e, 47.20.Ma, 47.65.+a, 47.15.Hg

I. INTRODUCTION

Liquid films are used in numerous technological applications such as coating and cooling processes—see, for example [1–6], where it is observed that the presence of waves on the interface can enhance the cooling ability of the system by an order of magnitude. There have been numerous studies of falling film problems at both small and intermediate Reynolds numbers, which aim to derive long wave nonlinear evolution equations for the interfacial motion—see the reviews by [7,8]. The effects of a vertical electric field have been added recently by [9,10] when the Reynolds numbers are small (see also [11]).

In the present work we concentrate on inviscid flows with the aim of establishing a fundamental understanding of the nonlinear processes involved in classical water wave theories when gravity, surface tension and electric field effects compete. To this end we assume that the fluid layer is a perfect dielectric of constant permittivity $\epsilon_p\epsilon_0$ and that of the air above it has constant permittivity ϵ_0. The effect of an electric field on dielectric liquid sheets has been studied analytically using a long wave theory in [12,13] for symmetric nonlinear undulations; further asymptotic and full numerical simulations based on boundary integral methods have been carried out in [14,15] for symmetric and antisymmetric traveling waves of arbitrary amplitude and wavelength. It was shown in [14] that the long wave theory performs very well as compared to the direct simulations, thus lending additional significance to the study of such nonlinear models. The orientation of the background electric field with respect to the unperturbed interface plays an important role on the ensuing dynamics. For example, when the field is horizontal (that is it acts in the plane of the unperturbed liquid-air interface), it provides a dispersive contribution to the linear dynamics and as found in the inviscid study of [12], a large initial disturbance is required to cause film rupture in finite time. When viscosity is present and the field is horizontal, a disjoining pressure must be included to allow for rupture (see [13]). The situation is quite different when the field is vertical to the interface; the electric field can now provide energy to certain ranges of wavenumbers and either enhance an existing instability, or allow for instability when none is present to begin with. This is true for both viscous [9,10] and inviscid problems, the latter being the subject of the present study. The physical mechanism by which an instability is produced, is connected with the drop in pressure induced by the electric Maxwell stresses just below an interfacial protrusion. This lowers the pressure relative to regions away from the disturbance and causes more fluid to be drawn in the vicinity of the perturbation, thus enhancing the instability. Our objective is to follow such initial dynamics into the fully nonlinear regime and in particular to identify regions in parameter space, which support nonlinear traveling waves or lead to rupture in finite time.

The outline of the article is as follows. In Sec. II the mathematical problem is formulated, nondimensionalized and its linear stability determined. In Sec. IV we carry out an asymptotic analysis invoking a long wavelength approximation and choosing scalings to retain gravity, surface tension and electrostatics; this leads to a system of coupled nonlinear and nonlocal evolution equations for the interfacial shape and the leading order horizontal velocity in the liquid layer.

*Electronic address: depapa@oak.njit.edu
†Electronic address: peterp@oak.njit.edu
‡Electronic address: h010@uea.ac.uk

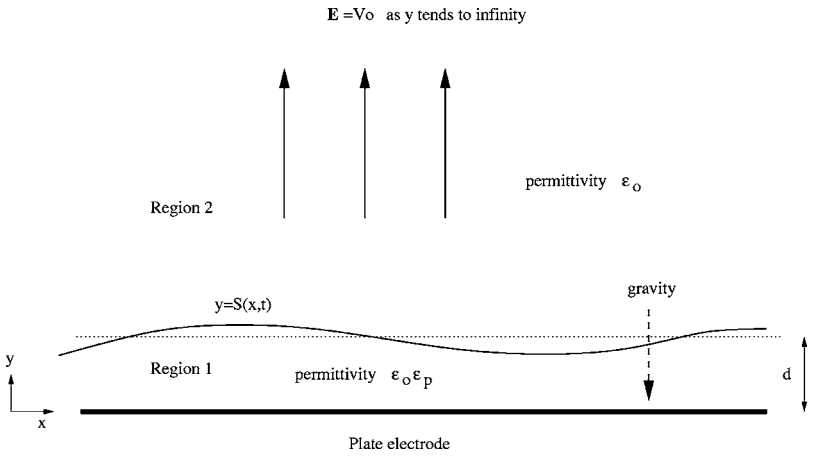

FIG. 1. Schematic of the problem.

In Sec. V we address the evolution equations numerically in two canonical cases: (i) For sufficiently weak fields nonlinear traveling waves are constructed and their stability investigated by solving appropriate perturbed initial value problems and (ii) for sufficiently strong electric fields where a band of unstable waves enters, we solve the initial value problem and present the generic evolution towards finite-time touchdown. In the latter case we also establish scaling laws for self-similar structures near the singular event. In Sec. VI we present our conclusions and comment on future work.

II. GOVERNING EQUATIONS

Consider a liquid layer of undisturbed thickness d lying on a horizontal plate electrode which is held at zero voltage. Using a Cartesian coordinate system fixed at the plate, we denote the plate by the x axis ($y=0$) and the undisturbed surface of the liquid layer by $y=d$. A constant electric field acts in the normal direction and the potential V far from the plate approaches V_{0y}, where V_0 is a constant. The bounding interface of the liquid layer is free to move and is defined by $y=S(x,t)$. We denote regions 1 and 2 by $0<y<S(x,t)$, and $y>S(x,t)$, respectively. The fluid in region 1 is assumed to be a perfect dielectric with permittivity $\epsilon_p\epsilon_0$, while region 2 is assumed to be hydrodynamically passive and of permittivity ϵ_0 (for example, region 2 could be air and ϵ_0 the permittivity of air—consequently in the formulation ϵ_p is the dimensionless permittivity ratio between regions 1 and 2). The geometry of the problem is sketched in Fig. 1.

The governing equations are the Laplace equations for the fluid potential ϕ and the voltage potentials $V^{(1)}$, $V^{(2)}$ in regions 1 and 2, respectively, along with electric field and stress boundary conditions at the moving interface (see, for example [12,14]). Variables are made dimensionless as follows: Lengths are scaled by d; pressures p are scaled by the hydrostatic value $\rho g d$ (ρ is the fluid density and g the acceleration due to gravity); velocities are scaled by $(gd)^{1/2}$, the fluid potential ϕ by $(gd^3)^{1/2}$, and time t by $(d/g)^{1/2}$; finally, voltages V are scaled by V_0.

The dimensionless governing equations are

Region 1

$$V^{(1)}_{xx} + V^{(1)}_{yy} = 0, \tag{1}$$

$$\phi_{xx} + \phi_{yy} = 0. \tag{2}$$

Region 2

$$V^{(2)}_{xx} + V^{(2)}_{yy} = 0. \tag{3}$$

There is a no penetration boundary condition at the solid boundary

$$\phi_y(x,0,t) = 0, \tag{4}$$

and at infinity the voltage matches the imposed value,

$$V^{(2)} \sim y, \quad y \to \infty. \tag{5}$$

The boundary conditions at the free surface $y=S(x,t)$ become

$$V^{(1)}_x + S_x V^{(1)}_y = V^{(2)}_x + S_x V^{(2)}_y, \tag{6}$$

$$\epsilon_p[V^{(1)}_y - S_x V^{(1)}_x] = V^{(2)}_y - S_x V^{(2)}_x, \tag{7}$$

$$-p_1 + p_2 + \frac{E_b}{(1+S_x^2)}\left(\frac{1}{2}(1-S_x^2)[\epsilon_p(V_y^2 - V_x^2)^{(1)} - (V_y^2 - V_x^2)^{(2)}] - 2S_x[\epsilon_p V_x^{(1)} V_y^{(1)} - V_x^{(2)} V_y^{(2)}]\right) = \frac{\tau S_{xx}}{(1+\delta^2 S_x^2)^{3/2}}, \tag{8}$$

$$\phi_y = S_t + \phi_x S_x. \tag{9}$$

The boundary conditions (6)–(9) represent continuity of tagential electric fields at the interface, continuity of the normal component of the displacement field ($\epsilon \nabla V$) there, continuity of the normal stress at the interface, and the kinematic condition. The parameters E_b and τ are an electric Bond number which is the ratio of electric to gravitational forces, and an inverse Bond number which is the ratio of capillary to gravitational forces, respectively,

$$E_b = \frac{\epsilon_0 V_0^2}{\rho g d^3}, \quad \tau = \frac{\sigma}{\rho g d^3}. \tag{10}$$

The parameter σ is the surface tension coefficient.

It is useful to eliminate the pressure difference $p_1 - p_2$ by using the Bernoulli equation

$$\phi_t + \frac{1}{2}(\phi_x^2 + \phi_y^2) + y = -p_1 + \text{const.}, \tag{11}$$

evaluated at $y=S$, and the normal stress balance (8), to obtain

$$\phi_t + \frac{1}{2}(\phi_x^2 + \phi_y^2) + S - 1 + \frac{E_b}{(1+S_x^2)}\left(\frac{1}{2}(1-S_x^2)[\epsilon_p(V_y^2 - V_x^2)^{(1)} - (V_y^2 - V_x^2)^{(2)}] - 2S_x[\epsilon_p V_x^{(1)} V_y^{(1)} - V_x^{(2)} V_y^{(2)}]\right) = \frac{\tau S_{xx}}{(1+S_x^2)^{3/2}} + \frac{E_b}{2}\left(\frac{1-\epsilon_p}{\epsilon_p}\right). \tag{12}$$

Prescription of initial and streamwise boundary conditions (e.g., periodicity in x) completes the general mathematical problem to be addressed for interfacial deviations of arbitrary wavelength and amplitude (see [14,15] for the horizontal electric field problem).

III. LINEAR STABILITY THEORY

The following is an exact solution of the governing equations and boundary conditions (overbars are used to denote unperturbed values):

$$\bar{S} = 1, \tag{13}$$

$$\bar{\phi} = 0, \tag{14}$$

$$\bar{V}^{(1)} = \frac{1}{\epsilon_p} y, \tag{15}$$

$$\bar{V}^{(2)} = y + \text{const.} \tag{16}$$

The constant in (16) can be set to zero without loss of generality—the equations and boundary conditions contain derivatives of the voltage alone. The base pressure distributions in regions 1 and 2 can be determined by substituting the solutions (15) and (16) into the normal stress balance condition (8). Denoting the pressure in region 2 by its ambient value p_a, we find

$$\bar{p}_1 = p_a + \frac{1}{2}\left(\frac{1-\epsilon_p}{\epsilon_p}\right)E_b. \tag{17}$$

Linear stability is analyzed by writing

$$\phi(x,y,t) = \zeta A e^{ikx+i\omega t}\cosh(ky) + \text{c.c.}, \tag{18}$$

$$V^{(1)}(x,y,t) = \bar{V}^{(1)}(y) + \zeta B e^{ikx+i\omega t}\sinh(ky) + \text{c.c.}, \tag{19}$$

$$V^{(2)}(x,y,t) = \bar{V}^{(2)}(y) + \zeta C e^{ikx+i\omega t}e^{-ky} + \text{c.c.}, \tag{20}$$

$$S(x,t) = \bar{S} + \zeta \eta_0 e^{ikx+i\omega t} + \text{c.c.}, \tag{21}$$

where c.c. denotes complex conjugates and the quantity $|\zeta| \ll 1$ is a linearization parameter. Substitution of (18)–(21) into the governing equations and linearization with respect to ζ leads to the following dispersion relation after some algebra:

$$\omega^2 = k\tanh(k) + \tau k^3 \tanh(k) - E_b\frac{(1-\epsilon_p)^2}{\epsilon_p}\frac{k^2}{1+\epsilon_p\coth(k)}. \tag{22}$$

In the absence of an electric field, $E_b=0$, the dispersion relation (22) is that for gravity capillary waves on a finite depth fluid layer; the waves are dispersive and have velocity c where

$$c^2 = \omega^2/k^2. \tag{23}$$

The electric field term is always negative (k is positive without loss of generality) and hence destabilizing. In Fig. 2 we show the dependence of the wave speed c^2 with wave number k for fixed values of $\tau=1$ and $\epsilon_p=2$, as E_b increases from zero. It can be seen that for nonzero but moderate values of E_b the waves remain dispersive; in addition there exists a wave number of zero group velocity. As E_b increases further, however, we find a unique value of E_b above which instability sets in. In Fig. 2 this value of E_b is between 10 and 15, and can be found by solving the following nonlinear algebraic equations for the neutral values k_c, E_{bc}:

$$c^2(k_c, E_{bc}) = 0, \quad \frac{\partial c^2}{\partial k}(k_c, E_{bc}) = 0. \tag{24}$$

Note that the neutral wave corresponding to $k=k_c$ has zero phase velocity and group velocity.

IV. LONG WAVE ASYMPTOTICS

We look for nonlinear solutions characterized by typical wavelengths which are long in comparison to their nonlinear amplitudes. Introducing a small parameter δ, we write

$$S(x,t) = \delta H(x,t), \quad H = O(1), \tag{25}$$

and seek asymptotic solutions of the governing equations in the limit $\delta \to 0$. The analysis that follows is similar to that of Papageorgiou and Vanden-Broeck [14] who derived long wave evolution equations in the case of a horizontal electric field. The fact that the electric field is acting vertically and is a linear function of y in its base state (as opposed to a linear function of x in [14]), can be dealt with in an elegant way by introducing conjugate harmonic functions. The function $V_x^{(1)} - iV_y^{(1)}$ is analytic in $z=x+iy$ and satisfies $V_x^{(1)}=0$ on $y=0$. We define the complex conjugate harmonic function $W_x^{(1)} - iW_y^{(1)}$ where

$$W_x^{(1)} = -V_y^{(1)}, \tag{26}$$

$$W_y^{(1)} = V_x^{(1)}. \tag{27}$$

It follows, then, that $W_x^{(1)} - iW_y^{(1)}$ is analytic in z and satisfies $W_y^{(1)}=0$ at $y=0$. Similarly, starting with $V_x^{(2)} - iV_y^{(2)}$ which is analytic in z, we obtain the analytic function $W_x^{(2)} - iW_y^{(2)}$, where

$$W_x^{(2)} = -V_y^{(2)}, \tag{28}$$

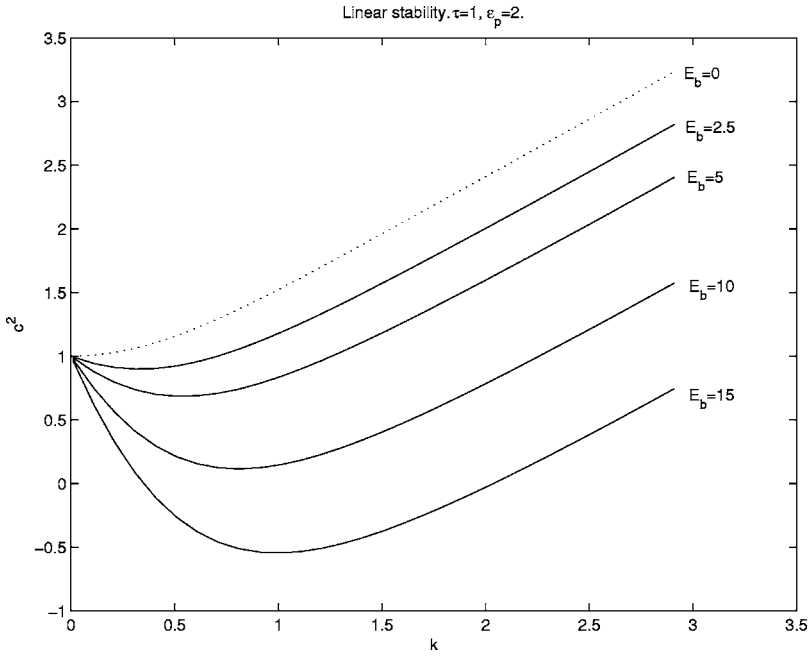

FIG. 2. Linear dispersion relation (22) as E_b varies. Here $\tau=1$ and $\epsilon_p=2$.

$$W_y^{(2)} = V_x^{(2)}. \tag{29}$$

The far-field condition $V_y^{(2)} \to 1$ as $y \to \infty$, is replaced by $W_x^{(2)} \to -1$ as $y \to \infty$. Making the substitutions (26)–(29) into the governing equations (1)–(3) and the boundary conditions (5)–(7) and (12), provides the following equivalent problem:

$$\nabla^2 \phi = 0, \quad \nabla^2 W^{(1,2)} = 0, \tag{30}$$

$$\phi_y(x,0,t) = 0, \quad W_y^{(1)}(x,0,t) = 0, \tag{31}$$

$$W_x^{(2)} \to -1 \quad \text{as} \quad y \to \infty. \tag{32}$$

The boundary conditions at the free surface $y=S(x,t)$ become

$$W_y^{(1)} - S_x W_x^{(1)} = W_y^{(2)} - S_x W_x^{(2)}, \tag{33}$$

$$\epsilon_p (W_x^{(1)} + S_x W_y^{(1)}) = W_x^{(2)} + S_x W_y^{(2)}, \tag{34}$$

$$\phi_t + \frac{1}{2}(\phi_x^2 + \phi_y^2) + S - 1 + \frac{E_b}{(1+S_x^2)}\left(\frac{1}{2}(1-S_x^2)[\epsilon_p (W_x^2 - W_y^2)^{(1)} - (W_x^2 - W_y^2)^{(2)}] - 2S_x[-\epsilon_p W_x^{(1)} W_y^{(1)} + W_x^{(2)} W_y^{(2)}]\right) = \frac{\tau S_{xx}}{(1+S_x^2)^{3/2}} + \frac{E_b}{2}\left(\frac{1-\epsilon_p}{\epsilon_p}\right). \tag{35}$$

The kinematic condition (9) remains unchanged and will be used later.

Using overbars to denote undisturbed states as before, an exact solution to the new system is given by a flat interface and

$$\bar{W}_x^{(1)} = -\frac{1}{\epsilon_p}, \quad \bar{W}_x^{(2)} = -1, \tag{36}$$

so in terms of the conjugate harmonic functions the field is horizontal in its undisturbed state. We introduce a stretched normal coordinate in region 1

$$\text{Region 1} \quad x \text{ unchanged}, \quad y = \delta Y, \tag{37}$$

$$\text{Region 2} \quad x \text{ unchanged}, \quad y \text{ unchanged}, \tag{38}$$

with Y an order one variable. The appropriate asymptotic expansions are

$$W^{(1)} = -\frac{1}{\epsilon_p} x + \delta W_1^{(1)} + O(\delta^3), \tag{39}$$

$$W^{(2)} = -x + \delta W_1^{(2)} + O(\delta^3), \tag{40}$$

$$\phi = \phi_0 + \delta^2 \phi_2 + \cdots, \tag{41}$$

$$S = \delta H_1 + \cdots. \tag{42}$$

Introducing the region 1 stretched variables into the governing Laplace equations (30), and applying the boundary conditions (31) at the solid surface $y=0$, gives the following leading order solutions

$$W_1^{(1)} = \Psi(x,t), \tag{43}$$

$$\phi_0 \equiv \phi_0(x,t), \tag{44}$$

$$\phi_2 = -\frac{1}{2} Y^2 \phi_{0xx}. \tag{45}$$

Using these solutions in the electrical boundary conditions (33) and (34) and noting that, to leading order, for region 2 variables the interface is at $y=0$, gives the following asymptotically correct conditions (see [14] for details):

$$W_{1y}^{(2)}|_{y=0} = \left(\frac{1-\epsilon_p}{\epsilon_p}\right) H_{1x}, \tag{46}$$

$$W_{1x}^{(2)}|_{y=0} = \epsilon_p \Psi_x. \tag{47}$$

The leading order contribution to the Bernoulli equation (35) is considered next using the solutions (43)–(45). It is convenient to differentiate (35) with respect to x first and to also use condition (47) to eliminate $W_{1x}^{(2)}|_{y=0}$ in favor of Ψ_x; the resulting asymptotically correct equation that retains inertia is

$$\phi_{0xt} + \phi_{0x}\phi_{0xx} + + \delta H_{1x} + \delta E_b(\epsilon_p - 1)\Psi_{xx} = \delta\tau H_{1xxx}. \tag{48}$$

A second equation involving ϕ_0 comes from the kinematic condition (9) which is of order δ at most and involves a contribution due to ϕ_1 also. This is

$$H_{1t} + (\phi_{0x} H_1)_x = 0. \tag{49}$$

It remains to determine the function $\Psi(x,t)$ in order to close the system. To achieve this we need to solve for the voltage potential in the elliptic region 2 and use boundary condition (46). One way to determine Ψ is to consider the function $F = W_{1x}^{(2)} - iW_{1y}^{(2)}$ which is analytic in $z = x + iy$, and to apply Cauchy's theorem to this function over a rectangular contour bounding region 2 with the upper part of the contour located at $y = y_0$. As $y_0 \to \infty$ then $F \to 0$, and the contributions over the vertical parts of the contour vanish due to periodicity (for presentation purposes it is easier to apply the theorem on a region $-\infty < x < \infty$ and apply periodicity at the end). Taking the limit $y \to 0$ gives

$$PV\int_{-\infty}^{\infty} \frac{W_{1x}^{(2)}(\mu,0) - iW_{1y}^{(2)}(\mu,0)}{\mu - x} d\mu = i\pi[W_{1x}^{(2)}(x,0) - iW_{1y}^{(2)}(x,0)], \tag{50}$$

where PV denotes the principal part of the integral. Taking the imaginary part of (50) and using the fact that $W_{1x}^{(2)}(x,0) = \epsilon_p \Psi_x$ [see (47)], together with the result (46) to eliminate $W_{1y}^{(2)}(x,0)$, gives

$$\Psi_x = -\left(\frac{1-\epsilon_p}{\epsilon_p^2}\right)\frac{1}{\pi} PV\int_{-\infty}^{\infty} \frac{H_{1x}}{\mu - x} d\mu. \tag{51}$$

Substituting this into the Bernoulli relation (48) and writing $u = \phi_{0x}$ gives

$$u_t + uu_x + \delta H_{1x} + E_b\left(\frac{1-\epsilon_p}{\epsilon_p}\right)^2 \left\{\frac{1}{\pi} PV\int_{-\infty}^{\infty} \frac{\delta H_{1xx}(\mu,t)}{\mu - x} d\mu\right\} = \delta\tau H_{1xxx}. \tag{52}$$

The nonlocal term in (52) is the Hilbert transform operator defined by

$$\mathcal{H}(f) = \frac{1}{\pi} PV\int_{-\infty}^{\infty} \frac{f(\mu)}{\mu - x} d\mu, \tag{53}$$

and on periodic domains it takes the form

$$\mathcal{H}_{per}(f) = \int_0^1 \cot(\pi(\mu - x)) f(\mu) d\mu. \tag{54}$$

Some well-known properties of these transforms used below are their symbols in Fourier space and the commutation property between the transform and derivatives, i.e. $[\mathcal{H}(f)]_x = \mathcal{H}(f_x)$. Finally we cast the two evolution equations in terms of the original variables (equivalently, scale δ out of the problem) to obtain the evolution system

$$u_t + uu_x + S_x + E_b\left(\frac{1-\epsilon_p}{\epsilon_p}\right)^2 \mathcal{H}(S_{xx}) = \tau S_{xxx}, \tag{55}$$

$$S_t + (uS)_x = 0. \tag{56}$$

Next, we show that the dispersion relation of the system (55) and (56) is identical to that of the full problem when the limit $k \ll 1$ is taken in (22). Writing $u(x,t) = \hat{u}\exp(ikx + i\omega t)$, $S = 1 + \hat{S}\exp(ikx + i\omega t)$, linearizing with respect to hat variables and using the fact

$$\mathcal{H}(e^{ikx}) = \frac{1}{\pi} PV\int_{-\infty}^{\infty} \frac{e^{ik\mu}}{\mu - x} d\mu = i\,\mathrm{sgn}(k) e^{ikx}, \tag{57}$$

gives the dispersion relation

$$\omega^2 = k^2 + \tau k^4 - E_b\left(\frac{1-\epsilon_p}{\epsilon_p}\right)^2 k^3. \tag{58}$$

This is identical to the small k expansion of (22) that keeps the leading order contribution from each of the three terms in (22).

It remains to formulate the asymptotic model into the computational format of traveling waves. We write

$$u = c + U, \quad \frac{\partial}{\partial t} \equiv 0, \tag{59}$$

to find

$$cU_x + UU_x + S_x + E_b\left(\frac{1-\epsilon_p}{\epsilon_p}\right)^2 \mathcal{H}(S_{xx}) = \tau S_{xxx}, \tag{60}$$

$$cS_x + US_x + U_x S = 0. \tag{61}$$

The speed for linear waves follows by linearization of (60) and (61), or equivalently from (58), as

$$c^2 = \frac{\omega^2}{k^2} = 1 + \tau k^2 - E_b\left(\frac{1-\epsilon_p}{\epsilon_p}\right)^2 k. \tag{62}$$

The term independent of k is due to the inclusion of gravitational effects which were absent in the study of Papageorgiou and Vanden-Broeck [14]. A mentioned earlier, a vertical field induces instability at sufficiently large values of E_b since c can become complex then. In what follows we consider traveling waves when E_b is below such a threshold and also address the dynamic problem in the linearly unstable regime.

V. NUMERICAL SOLUTIONS

The numerical solution of (55) and (56) is carried out using a pseudospectral method in space and a standard four-

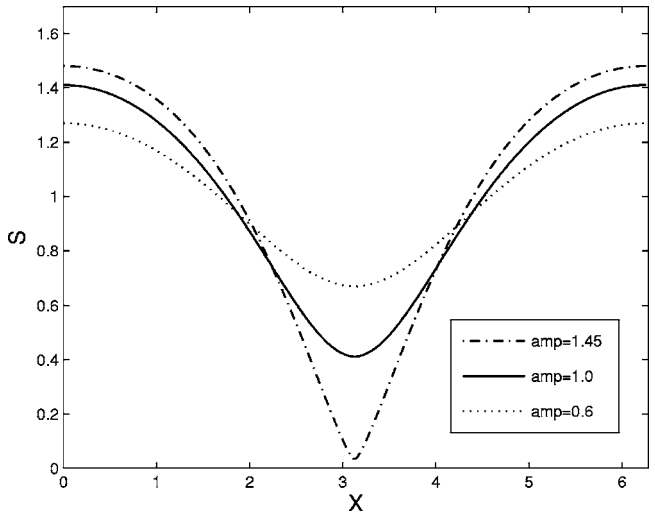

FIG. 3. Interfacial traveling wave profiles with speed $c=-0.825053$ (dotted line), $c=-0.73347$ (solid line), and $c=-0.31799$ (dash-dot line); $E_b=5$.

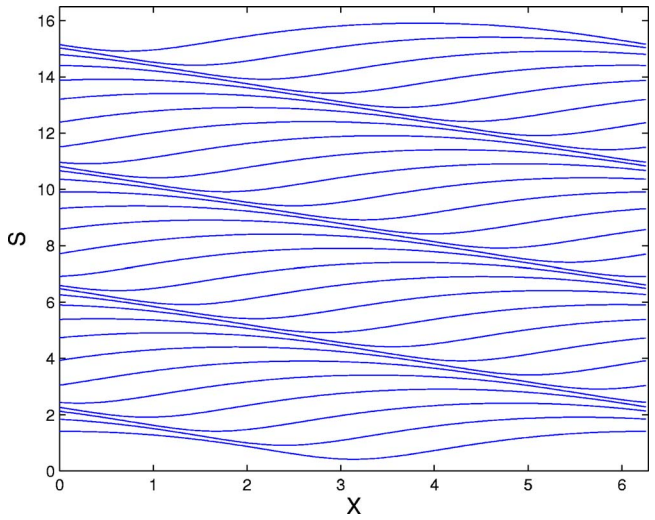

FIG. 4. (Color online) Stable unimodal wavetrain of amplitude 1 and speed $c=-0.73347$ under zero initial perturbation; $E_b=5$.

stage Runge-Kutta method in time. Spectral accuracy is maintained at all times during a computation by determining the time step and the number of spatial modes adaptively according to the evolution of the spatial spectrum of the solution. Details pertaining to our code can be found in [12,13]. The initial conditions are $S(x,0)=S(x)+h_0\cos(x)$ and $u(x,0)=U(x)+u_0\sin(x)$, where $S(x)$, $U(x)$ are either the computed traveling wave solutions or the flat film base state ($S=1$, $U=0$), and h_0, u_0 are prescribed perturbation amplitudes. To validate our code we propagated traveling waves (see below) over long time intervals and confirmed that the observed wavespeed matched that of the wave used as initial data in the simulation. All our numerical results were obtained with $\tau=1$ and $\epsilon_p=2$.

A. Traveling waves and their stability

When E_b is less than E_{bc}, the flat film state is linearly stable and dispersive, and nonlinear traveling waves are possible. For $E_b>E_{bc}$, however, traveling waves (if they exist) are unstable and as shown later, lead to the formation of a dry spot in finite time. In this section we consider $E_b<E_{bc}$.

Traveling wave solutions of the evolution equations (60) and (61) are calculated numerically by using a Newton iteration procedure. The unknowns are the values of U and S_x at the nodes of a regular grid, and these are used to construct approximations of U, U_x, S_{xxx} and S_x at another set of grid points which are shifted by half a mesh spacing with respect to the original grid. Also, S_{xx} is approximated by a four-point difference formula on the original grid. The Cauchy principle value integral (53) is evaluated using a trapezoidal rule with summation over the shifted grid nodes. The value of S at the shifted grid nodes is found by integration of S_x using as initial condition $S(0)=\alpha$, where α is the traveling wave amplitude. The resulting set of nonlinear equations is solved by Newton's method. For details of the method we refer to [14].

Figure 3 shows interfacial traveling wave profiles of increasing amplitude. It is observed that the wave speed decreases as the amplitude increases; in addition, for the largest amplitude used (1.45), the minimum film thickness is less than 0.01 and the local geometry near the minimum is wedge shaped. Our computations indicate that there exists a critical amplitude above which the traveling wave interface touches down, that is the minimum thickness becomes zero.

The stability of traveling waves is considered next. We solve the initial value problem for (55) and (56) with initial conditions given by traveling waves computed as described above. In Fig. 4 we show the evolution up to a computational time of 50 units, for the traveling waves with unit amplitude (solid line in Fig. 3), and no added perturbation. It is seen that the wave propagates without changing shape or speed and hence is stable in this sense. When a perturbation of amplitude $h_0=0.1$, $u_0=0$, is added to the interfacial traveling wave, the motion evolves dynamically with a quasiperiodic oscillation of the amplitude and corresponding horizontal velocity (not shown here). Evidence of this nonlinear stability is presented in Fig. 5 which depicts the minimum film thickness as a function of time up to 50 time units. Computations with other traveling wave profiles produce similar results, as long as the perturbation h_0 is sufficiently small. We have ran cases with large initial perturbations in the linearly stable regime, namely $E_b=5$, $h_0=0.8\cos(x)$, $u_0=0$ and $E_b=1.25$, $h_0=0.9\cos(x)$, $u_0=0$, in order to discover if touchdown can occur in the linearly unstable regime for large initial conditions. In both cases the response of the system is to produce persistent interfacial oscillations without rupture (the minimum film thickness is larger than roughly 0.2 and 0.1, respectively). It is possible, however, that rupture can occur if the initial conditions are carefully chosen by including a large initial perturbation in u_0 also. The question of the modulational stability of the nonlinear traveling waves to perturbations larger than that of the underlying period, is the subject of current work. It is interesting to note that the related problem in [12] exhibits such modulational instabilities.

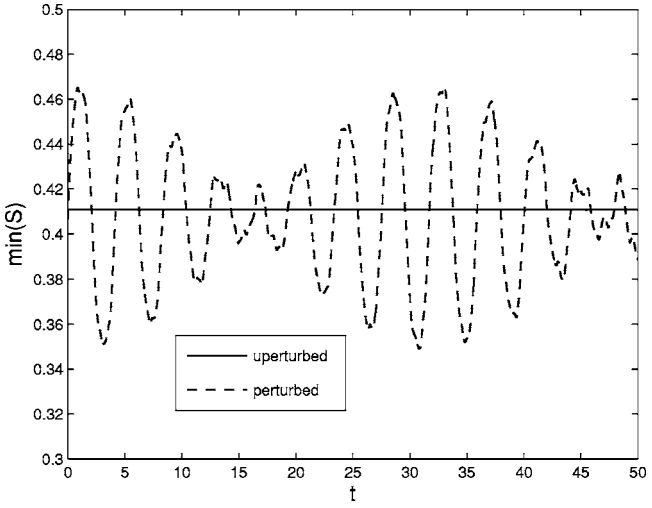

FIG. 5. Stability of unimodal interfacial traveling wave of amplitude 1: $h_0=u_0=0$ (solid line), $h_0=0.1$, $u_0=0$ (dashed line); $E_b=5$.

B. Time dependent solutions

The initial value problem is solved next when $E_b>E_{bc}$; all computations have $E_b=16$ and initial perturbations $h_0=0.1$ and $u_0=0$. The evolution to rupture of the interface is shown in Fig. 6, and the horizontal velocity at the last computed time $t=1.747076591$, is shown in Fig. 7. Numerical experiments with other initial perturbations lead to similar results. It is evident that the interface touches down in a finite time and the corresponding velocity becomes infinite near the touchdown points. It is possible to describe the dynamics near the singular time $t=t_s$ and singular point(s) $x=x_s$, in terms of the following similarity solutions:

$$S(x,t)=(t_s-t)^{\alpha}f\left(\frac{x-x_s}{(t_s-t)^{\beta}}\right),\quad u(x,t)=(t_s-t)^{\gamma}g\left(\frac{x-x_s}{(t_s-t)^{\beta}}\right), \tag{63}$$

where the exponents $\alpha>0$, $\beta>0$, $\gamma<0$ and the scaling functions f and g are to be determined. Substitution of the ansatz (63) into the governing equations (55) and (56), and a balance of most singular terms, provides two balance equations for the three unknown exponents; the similarity solution is therefore of the second kind with the exponents related by

$$\gamma=\beta-1,\quad \gamma-1=\alpha-3\beta. \tag{64}$$

The first expression comes from the dominant balance $u_t\sim uu_x\sim S_{xxx}$ and the second from $S_t\sim(uS)_x$. In order to determine the exponents we need to use the numerical results and extract information up to the singular time. Our calculations indicate that the minimum of S, S_{min} say, goes to zero linearly as t_s is approached. Plots of S_{min} against time are shown in Figs. 8 and 9; the latter plot considers the behavior near the singular time and superimposes a least squares linear fit. The fit is in turn used to estimate the singular time, $t=t_s$ by extrapolation. This linear behavior implies that $\alpha=1$ and then expressions (64) yield

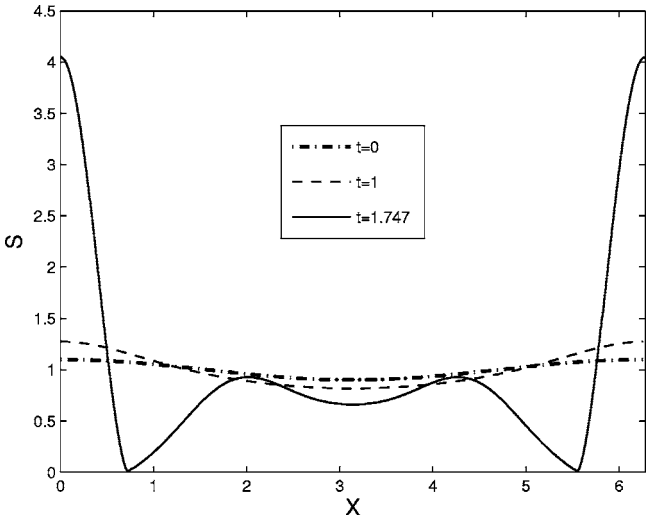

FIG. 6. Interfacial profile from initial conditions with $h_0=0.1$, $u_0=0$; $E_b=16$.

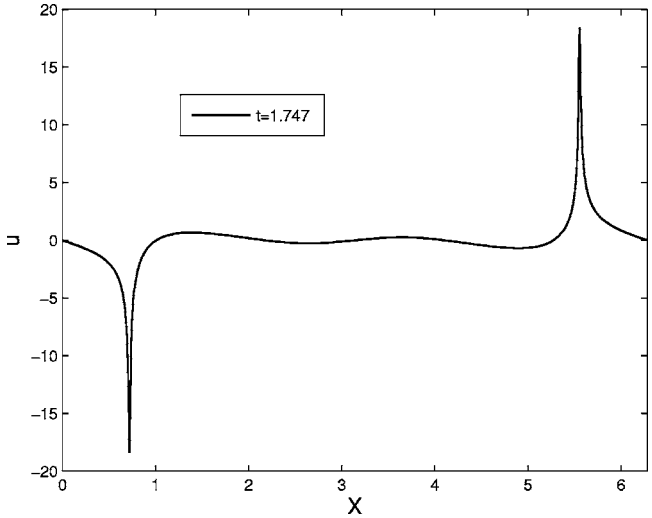

FIG. 7. Velocity profile near the time of pinching from initial conditions with $h_0=0.1$, $u_0=0$; $E_b=16$.

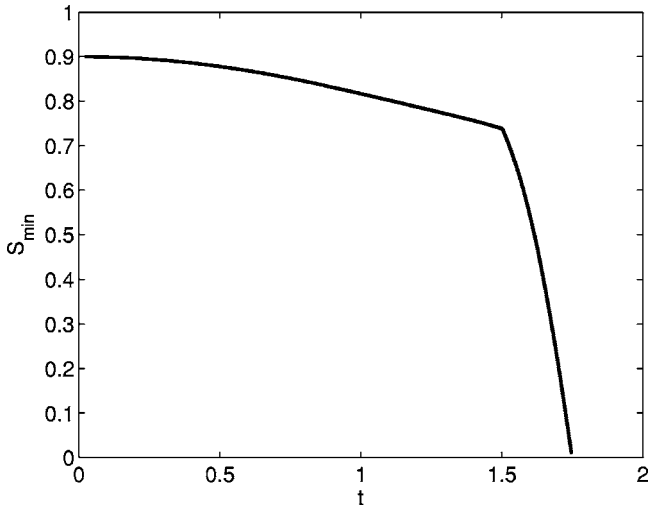

FIG. 8. Evolution of the minimum interface height from initial conditions with $h_0=0.1$, $u_0=0$; $E_b=16$.

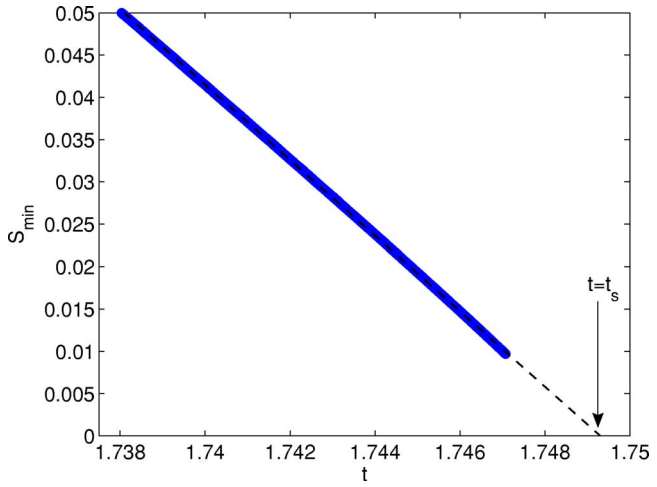

FIG. 9. (Color online) Final stage of the evolution of the minimum interface height from initial conditions with $h_0=0.1$, $u_0=0$; $E_b=16$. The dashed line indicates the least-squares fit to the computed data.

$$\alpha = 1, \quad \beta = \frac{1}{2}, \quad \gamma = -\frac{1}{2}. \tag{65}$$

Further numerical confirmation of these exponents has been carried out by consideration of the evolution of the maximum value of the velocity, u_{max} say. The evolution of u_{max} is shown in Fig. 10 which clearly shows the blow up in a finite time. To confirm the blow up rate of $(t_s-t)^{-1/2}$, we show in Fig. 11 the log-log plot of u_{max} against the time distance from the singularity, and estimate the slope to be −0.47, in reasonable agreement with the exact value of −0.5. We also note that according to the result (65), S_x and S_{xx} remain bounded near the touchdown point and this is supported by the calculations also. It is straightforward to obtain the nonlinear ODEs describing the scaling functions f and g, and this is not pursued further here. We note, however, that the shape of the

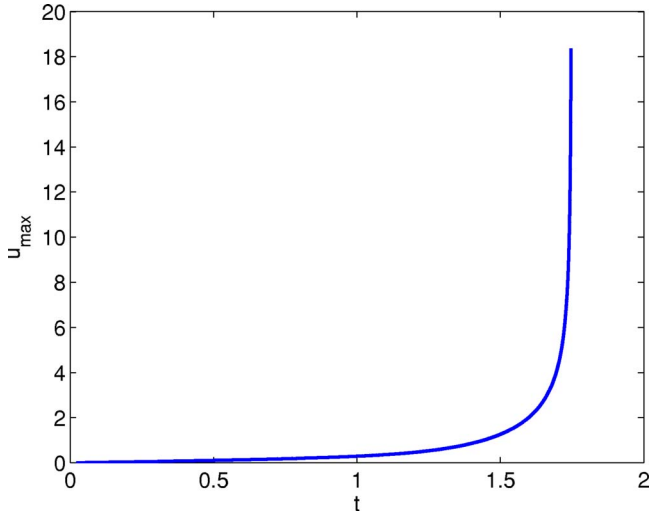

FIG. 10. (Color online) Evolution of the maximum horizontal velocity in the fluid layer from initial conditions with $h_0=0.1$, $u_0=0$; $E_b=16$.

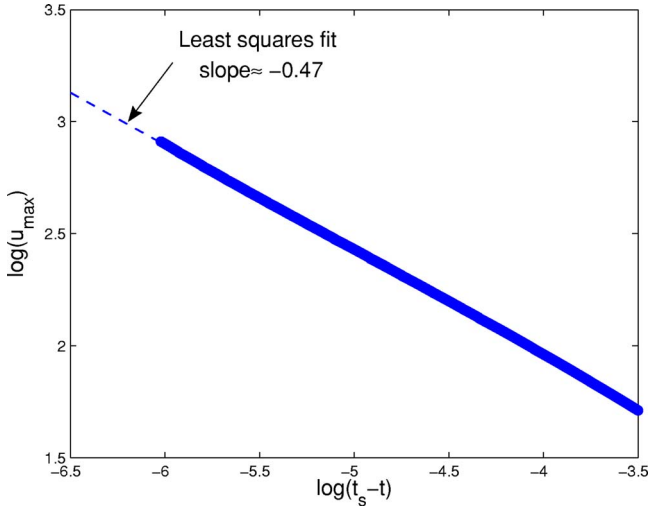

FIG. 11. (Color online) Final stage of the evolution of the maximum horizontal velocity in the fluid layer from initial conditions with $h_0=0.1$, $u_0=0$; $E_b=16$.

interface near the singular space-time point, is parabolic; this can be seen from the form of the interfacial scaling function $S \sim (t_s-t)f(\xi)$ where $\xi=(x-x_s)/(t_s-t)^{1/2}$ for large ξ. In this limit and far from the singular point, S is expected to behave quasistatically with respect to the fast time scale over which the singularity is taking place. This in turn implies that $f \sim \xi^2$ for $|\xi| \ll 1$, yielding a locally parabolic shape as viewed from outside the self-similar region. An analysis of the ODEs describing the scaling functions produces an identical result as well as the decay of the velocity scaling function according to $g \sim \xi^{-1}$ for large ξ.

These estimates are consistent with Eq. (64) and the approximation is expected to improve in computations which proceed to much smaller values of S_{min}—our computations possess only two decades of data due to the small time step and large number of modes required to resolve the singular structures.

VI. CONCLUSIONS

We have studied the nonlinear stability of a perfect dielectric liquid layer wetting a solid substrate electrode held at constant voltage. A second electrode is placed laterally far away so that the motion is driven by an initially piecewise constant vertical electric field which is uniform in the horizontal direction. Two regimes were identified: (i) $E_b < E_{bc}$ which provides linearly stable dispersive waves, and (ii) $E_b > E_{bc}$ which induces a band of unstable waves centered about a finite wave number $k=k_c$. The objective of this work is to follow initial dynamics into the nonlinear regime in both cases. This has been achieved by derivation of a coupled system of evolution equations for the interfacial position and the horizontal fluid velocity, valid for long waves. These equations are studied for traveling waves in case (i) where it is found that larger amplitude waves travel slower than smaller amplitude ones. Numerical computations indicate that these waves are stable to small perturbations of the

same wavelength as the traveling waves. When the vertical electric field induces a linear instability, our numerical computations provide strong evidence for interface touchdown (and local velocity blow up), according to a similarity solution of the second kind. The computations were used to extract scaling exponents. These are different from the work of [12] even though the governing equations are very similar and the main balances near the singularity are the same. This can be attributed to the existence of a second kind similarity solution which is sensitive to the different effects of the electric field and gravity in the present problem prior to the singularity, even though these become higher order effects near blow up. This work provides a computationally tractable model for singularity formation which can be of value to direct numerical simulations in the future.

ACKNOWLEDGMENTS

The work of D.T.P. and J.M.V.D.B. was supported by the National Science Foundation Grant No. DMS-0072228 and No. DMS-0204808. The work was also supported by EPSRC and NATO. The work of P.G.P. was supported by AFOSR Grant No. FA9550-05-1-0162.

[1] A. E. Dukler, Chem. Eng. Educ. **Summer 1976**, 108 (1976).
[2] P. N. Yoshimura, T. Nosoko, and T. Nagata, Chem. Eng. Sci. **51**, 1231 (1996).
[3] V. Bontozoglou, Int. J. Heat Mass Transfer **41**, 2297 (1998).
[4] T. Nagasaki, H. Akiyama, and H. Nakagawa, Therm. Sci. Eng. **10**, 1231 (2002).
[5] K. Serifi, N. A. Malamataris, and V. Bontozoglou, Int. J. Therm. Sci. **43**, 761 (2004).
[6] G. A. Sisoev, O. K. Matar, and C. J. Lawrence, Chem. Eng. Sci. **60**, 827 (2005).
[7] H.-C. Chang, Annu. Rev. Fluid Mech. **26**, 103 (1994).
[8] H.-C. Chang and E. A. Demekhin, *Complex Wave Dynamics on Thin Films* (Elsevier, Amsterdam, The Netherlands, 2002).
[9] A. Gonzalez and A. Castellanos, Phys. Rev. E **53**, 3573 (1996).
[10] D. Tseluiko and D. T. Papageorgiou (unpublished).
[11] H. Kim, S. G. Bankoff, and M. J. Miksis, Phys. Fluids A **4**, 2117 (1992).
[12] B. S. Tilley, P. G. Petropoulos, and D. T. Papageorgiou, Phys. Fluids **13**, 3547 (2001).
[13] K. Savettaseranee, D. T. Papageorgiou, P. G. Petropoulos, and B. S. Tilley, Phys. Fluids **15**, 641 (2003).
[14] D. T. Papageorgiou and J.-M. Vanden-Broeck, J. Fluid Mech. **508**, 71 (2004).
[15] D. T. Papageorgiou and J.-M. Vanden-Broeck, Eur. J. Appl. Math. **15**, 609 (2005).